BEILSTEIN ARCHIVES

Preprint Title	Nanocarrier containing carboxylic and histamine groups with dual action: acetylcholine hydrolysis and antidote Atropine delivery
Authors	Elina E. Mansurova, Andrey A. Maslennikov, Anna P. Lyubina, Alexandra D. Voloshina, Irek R. Nizameev, Marsil K. Kadirov, Albina Y. Ziganshina and Igor S. Antipin
Publication Date	11 Juli 2024
Article Type	Full Research Paper
Supporting Information File 1	SI.pdf; 440.9 KB
ORCID® iDs	Irek R. Nizameev - https://orcid.org/0000-0002-5420-6181; Albina Y. Ziganshina - https://orcid.org/0000-0003-4507-9923

Nanocarrier containing carboxylic and histamine groups with dual action: acetylcholine hydrolysis and antidote Atropine delivery

Elina E. Mansurova[1,2], Andrey A. Maslennikov[2], Anna P. Lyubina[1], Alexandra D. Voloshina[1], Irek R. Nizameev[3], Marsil K. Kadirov[1,4], Albina Y. Ziganshina*[1] and Igor S. Antipin[2]

Address: [1] A. E. Arbuzov Institute of Organic and Physical Chemistry, FRC Kazan Scientific Centre, Russian Academy of Sciences, Arbuzov str. 8, Kazan 420088, [2] Alexander Butlerov Institute of Chemistry, Kazan Federal University, Lobachevsky str. 1/29, Kazan 420008, [3] Kazan National Research Technical University named after A.N. Tupolev - KAI, 10, K. Marx str., Kazan 420111 and [4] Kazan National Research Technological University, 68, K. Marx str., Kazan 420015

Email: Albina Y. Ziganshina – az@iopc.ru

* Corresponding author

Abstract

Disruption of cholinesterases and, as a consequence, increased levels of acetylcholine lead to serious disturbances in the functioning of the nervous system, including death. The need for rapid administration of an antidote to restore esterase activity is critical, but practical implementation of this is often difficult. One promising solution may be the development of antidote delivery systems that will release the drug only when

acetylcholine levels are elevated. This approach will ensure timely delivery of the antidote and minimize side effects associated with uncontrolled drug release. Here, we describe the creation of a new smart system that serves as a carrier for delivering an antidote (atropine) and functions as a synthetic esterase to hydrolyze acetylcholine. The nanocarrier was synthesized through microemulsion polycondensation of phenylboronic acid with resorcinarenes containing hydroxyl, imidazole, and carboxylic groups on the upper rim. The nanocarrier breaks down acetylcholine into choline and acetic acid. The last one acts on boronate bonds, dissociating them. It leads to the destruction of the nanocarrier and the release of the antidote. The paper covers the creation of the nanocarrier, its physicochemical and biological properties, encapsulation of the antidote, acetylcholine hydrolysis, and antidote release.

Keywords

Antidote delivery; atropine; nanocarrier; resorcinarene; acetylcholine, artificial cholinesterase

Introduction

Cholinergic toxicity results from an excessive quantity of acetylcholine (ACh), causing muscle cramps, nausea, vomiting, and other serious issues [1]. ACh overproduction usually results from a malfunction of the cholinesterase enzyme caused by poisoning or medication used [2, 3]. Drug dosage regulation can greatly lower cholinergic toxicity [4], but the risks associated with poisoning are far higher. Poisons cause permanent disruptions to cholinesterases function. Organophosphorus compounds (OPs) are among these toxins [5]. This class of chemicals finds application in the manufacturing of insecticides, medications, rubber, plastics, paints, and other products. However, if

used improperly, the majority of them can have a nerve-paralyzing impact and have major health repercussions. The irreversible binding of OPs to the cholinesterase receptors renders the enzyme completely inactive. An antidote that counters the effects of the OPs on the enzyme is given to treat OPs poisoning. Atropine (Atr) [6-8], an alkaloid used to regulate heart rate and treat eye ailments [9, 10], is one such antidote. Despite its advantages, Atr has limitations in OPs poisoning treatment. Firstly, it can be harmful in high doses, and timely administration is vital to prevent permanent damage. Additionally, Atr itself can inhibit cholinesterases, potentially causing increased ACh levels. Developing nanocarriers for Atr delivery could provide a solution. These carriers might improve the efficacy of Atr, prolong its action duration, and reduce its toxicity [11, 12].

In recent years, resorcinarenes, which are analogues of calixarenes, have been extensively utilized in the creation of different smart systems [13, 14]. Owing to their unique structural features, these macrocycles are employed in catalysis, such as in the breakdown of OPs [15-18], as carriers for drug delivery [19-22], and in the creation of diverse receptors and sensors, notably for ACh [23-27].

Here, we report the development of a new nanocarrier that can both carry Atr and act as a synthetic esterase to degrade excess ACh. The nanocarrier was synthesized via microemulsion polycondensation of phenylboronic acid with resorcinarenes containing carboxylic, imidazole, and hydroxylic groups on the upper rim. Similar to the esterase triad, these groups are essential for the hydrolysis of ACh [28]. Throughout hydrolysis, ACh dissociates into choline (Ch) and acetic acid (AcOH). The generated AcOH triggers the boronate bonds disintegrating of the nanocarrier, leading to the release of Atr (Scheme 1). This paper discusses the synthesis of the Atr nanocarrier, its physicochemical and biological properties, the encapsulation of Atr into

the nanocarrier cavity, ACh hydrolysis, nanocarrier degradation, and Atr release under the ACh action.
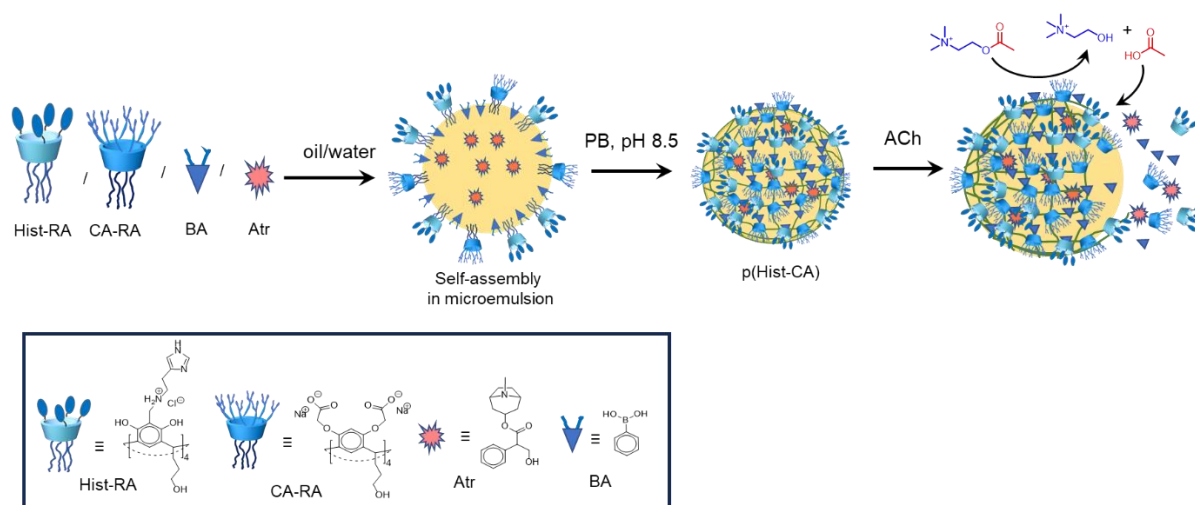
Scheme 1: Synthesis of Atr@p(Hist-CA) and Atr release following ACh hydrolysis.

Results and Discussion

Synthesis of the nanocarrier p(Hist-CA)

For the development of the Atr nanocarrier, two resorcinarenes were selected: one with carboxylate groups (CA-RA) and the other with hydroxylic and imidazole groups (Hist-RA, Scheme 1). CA-RA was obtained according to [29]. Hist-RA was synthesized by a Mannich reaction from resorcinarene with propanolic groups on the lower rim (RA), formaldehyde, and histamine in two steps, similar to those described in [30, 31]. The yield was 41%. The spectral data of CA-RA and Hist-RA are detailed in the experimental section and are present in Figures S1 and S2 of the Supporting Information (SI).

The nanocarrier (p(Hist-CA)) was prepared using the microemulsion technique [32, 33] through the condensation of CA-RA and Hist-RA with phenylboronic acid (BA) in phosphate buffer (PB) at pH 8.5 [34, 35]. CA-RA and Hist-RA are amphiphilic

4

molecules. Within a microemulsion system, they self-assemble at the interface, between water and oil. The hydrophilic groups face the aqueous phase, while the resorcinarene scaffold with tails on the lower rim points towards the dispersed (oil) phase. Under slightly basic conditions (pH 8.5), resorcinarenes react with BA to form boronate esters through cross-linking (Scheme 1).

To synthesize p(Hist-CA), 4 mL of BA solution (1.25 mM) in PB pH 8.5 and 7.3 µL of triolein (TO) were added to a mixture of Hist-RA (2 mM) and CA-RA (4.4 mM) in 1 mL of water. The mixture was vortexed for 1.5 minutes until an emulsion formed. Subsequently, the emulsion underwent homogenization in an ultrasonic bath while being blown with argon for 1.5 hours to generate a uniformly dispersed solution. Polycondensation occurred at 25°C for 3 days with stirring. p(Hist-CA) was then purified through dialysis during 1.5 hours using a 12,000 Da pore dialysis bag. The size of p(Hist-CA) is approximately 12 ± 3 nm according to the TEM image, and it forms aggregates ranging in size from 80 to 150 nm (Figure 1a,b).

The particle distribution diagram from DLS data displays two peaks with average hydrodynamic diameter 50 nm and 190 nm (Figure 1c). Evidently, the first one corresponds to the hydrodynamic diameter of p(Hist-CA), while the second relates to the aggregate size. The average molecular weight (M) of the aggregate was determined using static light scattering (SLS) Debye plot. The plot of KC/R_θ against C, where K is the Debye constant, C is the concentration, and R_θ is the Rayleigh ratio, intersects the ordinate at $1/M$, measuring 0.405±0.125 1/MDa. This implies M equals 2750±800 kDa (Figure 1d).
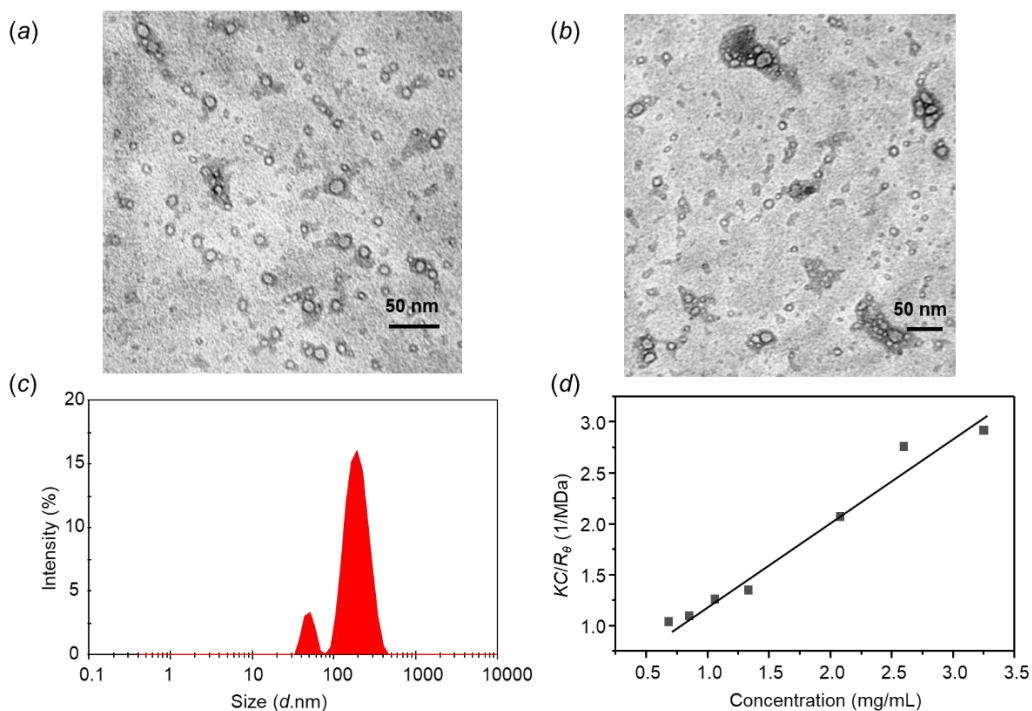
Figure 1: Data for p(Hist-CA): (*a*, *b*) TEM images, and (*c*) distribution diagram of the hydrodynamic diameter, C = 2 mg/mL and (b) Debye plot, C = 0.6–3.3 mg/mL, H_2O, 25 °C.

In the IR spectrum, bands of O-H and N-H stretching vibrations of p(Hist-RA) appear at 3700 – 3100 cm^{-1} (Figure 2). The C-H bond exhibits wild stretching vibration bands at 2700 – 3000 cm^{-1}. A vibration of C=O is fixed at 1744 cm^{-1}. Stretching of C-C in aromatic rings is evident at 1610 and 1501 cm^{-1}. The p(Hist-RA) IR spectrum also exhibits boronate bond stretching bands at 1066 and 543 cm^{-1}, which are not present in the Hist-RA and CA-RA spectra (Figure 2).
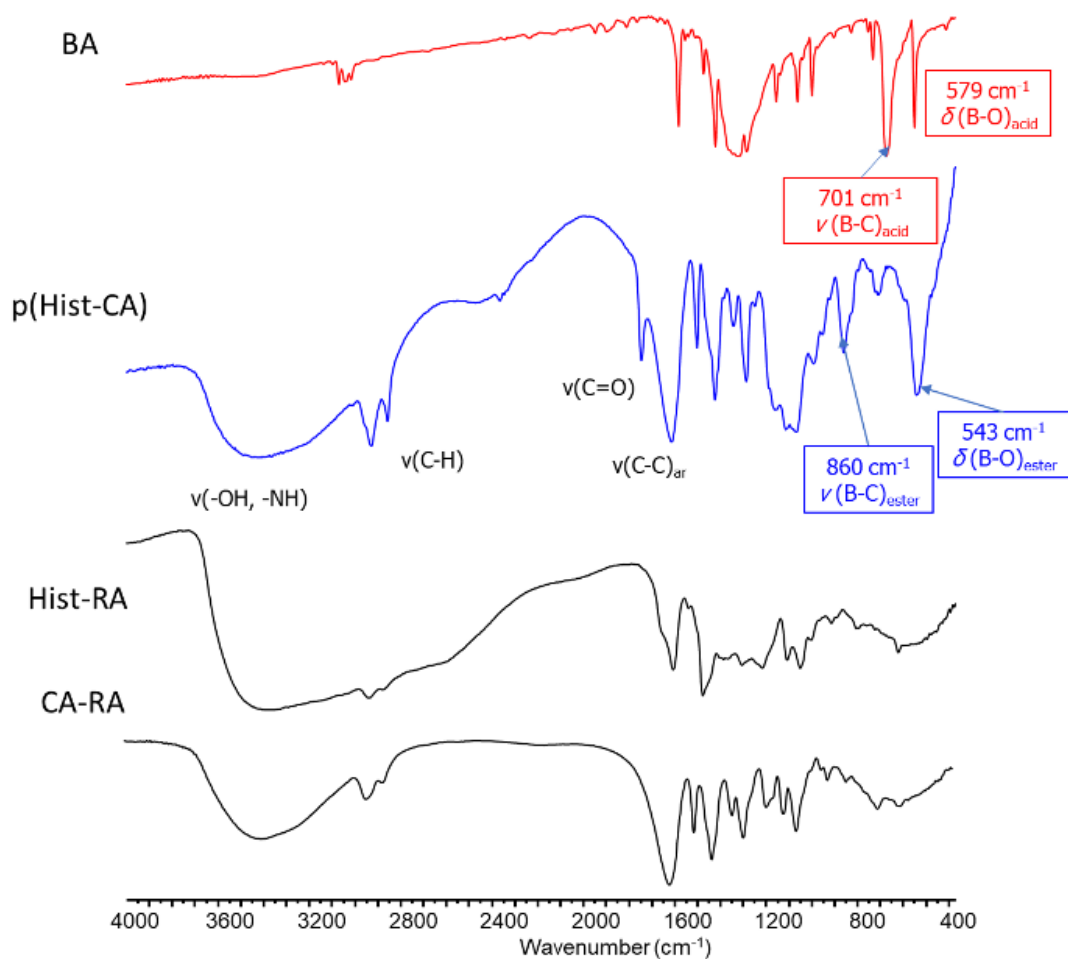
Figure 2: IR spectra of BA, p(Hist-CA), Hist-RA and CA-RA in KBr.

Cytotoxicity and hemocompatibility

According to the cytotoxicity investigation, Hist-CA, Hist-RA, and CA-RA are all found to be low-toxic. Hist-RA shows an IC_{50} of greater than 0.22 mM for the WI38 human embryonic lung cell line and the Chang Liver human liver cell line (Table 1). The IC_{50} values for CA-RA are 0.57 mM and 0.48 mM for WI38 and Chang Liver, respectively. For these cell lines, p(Hist-CA) has an IC_{50} higher than 1.4 mg/mL (Table 1).

Table 1: IC_{50} for Hist-RA, CA-RA and p(Hist-CA), obtained on the healthy Chang liver cell line and WI38 human embryonic lung cell line.[a]

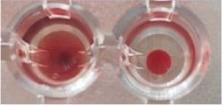|	IC_{50}		HC_{50}
	Chang Liver	WI38	
Hist-RA	>220 µM	>220 µM	177 µM
CA-RA	571±48 µM	479±37 µM	>528 µM
p(Hist-CA)	1.48±0.06 mg/mL C(Hist-RA) = 196±7 µM C(CA-RA) = 392±15 µM	1.75±0.24 mg/mL C(Hist-RA) = 232±32 µM C(CA-RA) = 464±64 µM	> 1.66 mg/mL C(Hist-RA) > 220 µM, C(CA-RA) > 440 µM

[a]The experiments were performed in triplicate. Results are expressed as the mean ± standard deviation (SD)

The agglutination activity results are shown in Figure 3. Control plate wells with erythrocytes in saline exhibited a dense layer at the bottom, indicating no agglutination (K(-), Figure 3). Positive control (K(+), Figure 3) displayed agglutinated cells (mixture of erythrocytes of blood groups IV and II) evenly distributed in the well.

The results revealed that CA-RA exposure to blood samples did not induce agglutination across a wide concentration range (13 - 1650 µM) and did not cause hemolysis even at the highest concentration of 825 µM (Table 1, Figure S3). Hist-RA at 220 µM led to nearly 100% hemolysis (Figure S3), while at concentrations of 110 and 55 µM, agglutination was observed (Figure 3). With further dilution, no erythrocyte effects were noted, as confirmed by bright-field microscopy data (Figure 4).

Nanocarrier p(Hist-CA) induces hemolysis (27.1 %) and agglutination solely at the highest concentration (Figures 3, S3).

	Starting Concentration	Dilution X times						
		X = 2	X = 4	X = 8	X = 16	X = 32	X = 64	X = 128
Hist-RA	440 µM							
CA-RA	1650 µM							
p(Hist-CA)	3.32 mg/mL C(Hist-RA) = 440 µM C(CA-RA) = 880 µM							

K(+)   K(-)

Figure 3: Agglutination assay. Blood samples is observed in the plate wells following the addition of diluted solutions of Hist-RA, CA-RA, and p(Hist-CA) at 2-128 folds dilution.

Hist-RA (220 µM) (hemolysis)	Hist-RA (110 µM) (agglutination)	Hist-RA (55 µM) (agglutination)
Hist-RA (25.5 µM) (no agglutination and hemolysis)	K (+)	K (-)

Figure 4: Bright-field microscopy (Nikon Eclipse Ci, 400x magnification). K (-) for intact cells; K (+) for the agglutination control.

Fluorescein encapsulation and release under the influence of ACh

To verify the degradation of p(Hist-CA) by ACh, fluorescein (Fl) was encapsulated into the nanocarrier cavity. Initially, 5 mg of Fl was dissolved in 15-20 mL of ethanol. Next, 7.3 μL of TO was added to the solution, and it was homogenized for 10 minutes in an ultrasonic bath. The solvent was then removed under reduced pressure. Then the solutions of Hist-RA (2 mM, 1 mL), CA-RA (4 mM, 1 mL), and BA (5 mM, 3 mL, PB pH 8.5) were added, and then the synthesis was carried out in a manner similar to that of p(Hist-CA). After the reaction, dialysis was carried out using a 12,000 Da dialysis bag to remove unencapsulated Fl, resulting in a solution of Fl@p(Hist-CA). The encapsulation efficiency (*EE*%) was found to be 55.2%.

In the UV spectra of Fl@p(Hist-CA) (PB pH 7.4), a hypsochromic shift in absorption typical of Fl in organic solvents is observed, confirming Fl location in the organic core. The rise in baseline indicates dispersed media (Figure 5a).

In fluorescence spectra (PB pH 7.4), the emission intensity of Fl@p(Hist-CA) is notably lower than that of free Fl due to self-quenching in a confined core and light screening by the polymer shell. The addition of glucose (5 mM) does not result in significant changes, suggesting the stability of Fl@p(Hist-CA) at typical glucose and pH levels.
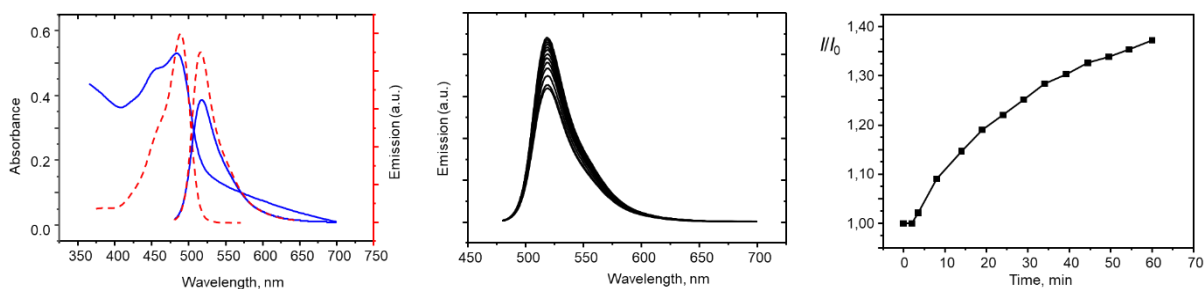
Figure 5: (*a*) UV and fluorescence spectra of Fl (red dotted line) and Fl@p(Hist-CA) (blue line), (*b*) Fluorescence spectra of Fl@p(Hist-CA) after the addition of ACh over time, and (*c*) Relative change in emission intensity of Fl@p(Hist-CA) at 517 nm over time; C(Fl) = 0.01 mM; C(ACh) = 0.1 mM; PB pH 7.4, 37 °C.

Atr encapsulation and release under the influence of ACh

Finally, Atr, the antidote for OPs poisoning, was inserted into p(Hist-CA). The process involved a reaction similar to that with Fl, but with Atr (10 mg) substituting Fl. Subsequently, polycondensation was carried out following the original procedure. After the polycondensation, the solution underwent dialysis for 1.5 hours employing a dialysis bag with 12000 Da pores to eliminate unencapsulated Atr. The resulting dialysate was then distilled under reduced pressure. The quantity of unencapsulated Atr was measured by NMR spectroscopy, applying 0.04% DMF in D_2O as a reference (Figure 6a). The amount of non-encapsulated Atr was determined by the ratio of the integral of the Atr methyl group signal at 5.05 ppm to the integral of the aldehyde group of DMF at 7.90 ppm. *EE*% was calculated as 60 %.
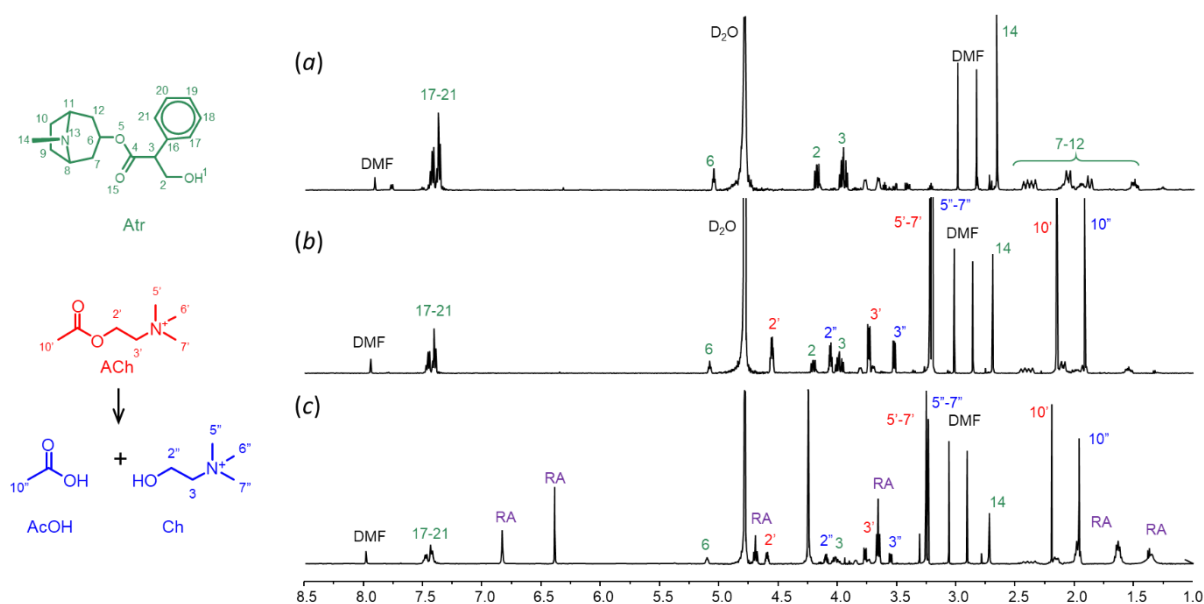
Figure 6: 1H NMR spectra for Atr@p(Hist-CA): (*a*) dialysate after synthesis of Atr@p(Hist-CA), (*b*) dialysate after addition of ACh, and (*c*) the rest of dialysing solution, C(ACh) = 5 mM, m(Atr) = 10 mg, PB pH 7.4, 37 °C.

Then, the polymer particles containing encapsulated Atr (Atr@p(Hist-CA)) were mixed with ACh (5 mM) before undergoing another round of dialysis for 1 hour. The dialysate was once again removed under reduced pressure, and the amount of Atr released in response to ACh was evaluated using NMR spectroscopy with 0.04% DMF in D_2O (Figure 6). The Atr release was 37.5 %.

In addition to the signals of Atr released, the ^{1}H NMR spectrum includes signals of ACh and its hydrolyzed products, Ch and AcOH. It confirms that ACh indeed undergoes hydrolysis by p(Hist-CA) (Figure 6b). In the ^{1}H NMR spectrum of the rest of the dialysis bag, both the signals from the broken-down nanocarrier and the signals of ACh, Ch, and AcOH are present (Figure 6c).

Conclusion

A polycondensation reaction of resorcinarenes with caboxylic and imidazole groups with phenylboronic acid in a microemulsion medium was utilized to create a nanocarrier

12

for acetylcholine hydrolysis and antidote delivery. Under healthy conditions, with a neutral pH and normal glucose concentrations, the nanocarrier is found to be stable. The employed resorcinarenes and the nanocarrier exhibit good hemocompatibility and low cytotoxicity with respect to human embryonic lung cells (WI38) and a healthy liver cell line (Chang Liver). The nanocarrier catalyzes the hydrolysis of acetylcholine into choline and acetic acid, which causes boronate bond dissociation and the subsequent nanocarrier destruction as was discovered by fluorescence and NMR spectroscopy.

Experimental

Equipment

Transmission electron microscopy (TEM) images were taken with a Libra 120 EFTEM (A Carl Zeiss SMT AG Company, Oberkochen, Carl Zeiss, Germany) at 100 kV. Samples were spread on a 300 mesh copper grid with a carbon/formvar support film. 1H and 13C NMR spectra were obtained using the Bruker Avance-600 spectrometer with an operating frequency of 600 MHz. Additionally, IR spectra were recorded using a Bruker Vector-22 Fourier transform spectrometer, with a range from 400 cm-1 to 4000 cm-1 in potassium bromide pellets. Elemental analysis was conducted using a CHNS analyzer EuroEA3028-HT-OM by Eurovector SpA (Italy). Samples were weighed on a Sartorius CP2P microbalance (Germany) in tin capsules. Quantitative measurements and data analysis were performed with Callidus 4.1 software. Hydrodynamic size and molecular weight were analyzed with a ZetaSizer Nano dynamic light scattering photon correlation spectrometer from Malvern, UK. Analysis was performed using Malvern dispersion technology software version 5.10. A Perkin-Elmer Lambda 25 UV-visible spectrometer was utilized for UV spectra collection. Fluorescence spectra were recorded on a HITACHI F 7100 spectrofluorometer.

Measurements were conducted at 37°C using a quartz cuvette that was 1×1×3.5 cm³ in size. The excitation wave was 475 nm, and the fluorescence spectra ware measured between 480 – 700 nm. Electronic analytical balances ViBRA AF-225 DRCE (220/0.001 g, resolution 0.00001 g) were utilized for weighing the samples. Ultrasonic treatment was performed with a "Sapfir" UZV 4.0 ultrasonic bath, operating at 280 W power and 35 kHz frequency. Mixing of the samples was conducted using a Multi Speed Vortex MSV-3500 Biosan. Phosphate buffer (PB) preparation followed the procedure outlined in [36]. RA was synthesized as described in [37].

Synthesis of Hist-RA
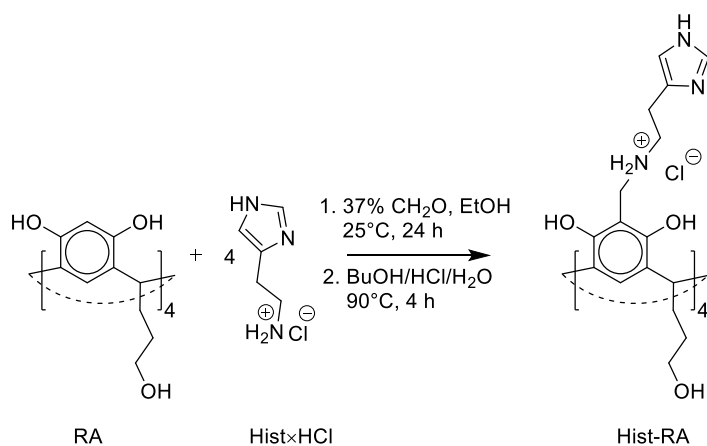
Histamine dihydrochloride (Hist×HCl, 0.66 g, 4.47 mmol) was dissolved in 10 mL of double-distilled water and adjusted to pH 10.75. The solvent was evaporated under reduced pressure, and the residue was dissolved in 10–15 mL of ethanol to obtain the Hist solution. In a 100 mL round-bottom flask, RA (0.53 g, 0.74 mmol) was dissolved in 20 mL of ethanol, and a 37% CH_2O solution (1.79 mL, 22 mmol) was added. Subsequently, the Hist solution was added, and the reaction mixture was stirred at room temperature for 24 h. Following this, the precipitate was filtered and washed with a cold ethanol/water mixture (9/1), which was then dissolved in 15 mL of butanol. After adding 1.5 mL of concentrated hydrochloric acid and 5 mL of double-distilled water, the mixture was stirred at 90 °C for 4 hours. The solution was then cooled to room

14

temperature, and 30 mL of chloroform was added. After evaporating the solvent under reduced pressure, 30 mL of diethyl ether was introduced, and the mixture was sonicated for 30 min. The product was subsequently filtered and washed with chloroform multiple times before being dried under reduced pressure at 80 °C for 2 hours. The yield is 0.42 g (42 %). ^{1}H NMR (600 MHz, D$_2$O) δ 1.55 (br., 8H), 2.29 (br., 8H), 3.14 (br., 8H), 3.69 (br., 16H), 4.49 (br., 8H), 5.36 (b., 4H), 7.57 (b., 4H), 8.75 (b., 8H). ^{13}C NMR (600 MHz, D$_2$O) δ 151, 134, 126, 124, 120, 108, 61, 46, 41, 39, 34, 30, 18. IR (KBr, cm^{-1}): 3500–3000, 2938, 1608, 1476. Anal. calcd for C$_{64}$H$_{88}$Cl$_4$N$_{12}$O$_{12}$: C, 56.55; H, 6.53; Cl, 10.43; N, 12.37; found: C, 56.48; H, 6.78; Cl, 10.20; N, 11.89;

Synthesis of CA-RA
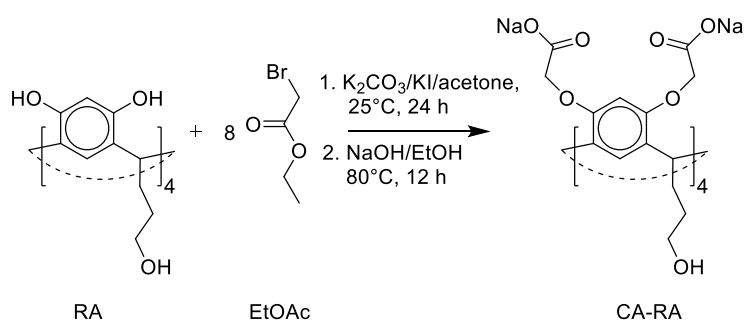
1. To a solution of 7 g (9.7 mmol) of RA in 100 ml of acetone, 10.74 g (77.6 mmol) of K$_2$CO$_3$ and 1.6 g (9.7 mmol) of KI were added. The mixture was stirred at room temperature, and a solution of ethyl bromoacetate (13 g, 77.8 mmol) in 100 ml of acetone was added dropwise. After addition, the mixture was stirred at 80 °C for 24 h, followed by the removal of the solvent under reduced pressure.

2. 50 ml of ethanol and 2 ml of 10 N NaOH were added to the oily residue. The mixture was heated at 80 °C for 12 h. The precipitate was filtered, washed with ethanol, and dried under reduced pressure. The yield is 8.3 g (63%). ^{1}H NMR (600 MHz, D$_2$O) δ 1.55 (m, 8H), 1.89 (q, 8H), 3.58 (t, 8H), 3.91 (s, 4H), 4.15 (s, 16H), 4.59 (t, 4H), 6.30 (s, 4H), 6.74 (s, 4H). ^{13}C NMR (600 MHz, D$_2$O) δ 174, 152, 124, 123, 98, 66, 59, 32,

27, 14. IR (KBr, cm^{-1}): 2938, 2866, 1608, 1334, 1501, 1423, 834. MALDI-TOF calcd for $C_{56}H_{62}O_{28}$: 1183; found: 1206 [M+Na+2H]; 1231 [M+2Na+2H]. Anal. calcd for $C_{56}H_{56}O_{28}Na_8$: C, 49.42; H, 4.15; Na, 13.51; found: C, 49.00; H, 3.98; Na, 13.91.

Synthesis of p(Hist-CA)

2.67 mg (2 µmol) of Hist-RA and 5.95 mg (4.4 µmol) of CA-RA were dissolved in 1 mL of double-distilled water. Subsequently, a solution of BA (0.6 mg, 5 µmol) in 4 mL of PB (pH 8.5) was added, along with 7.3 µL of TO. The mixture was vortexed at 3500 rpm for 1 min. Following this, the solution underwent argon purging and 90 min of sonication to homogenize the microemulsion. Then the emulsion was stirred at room temperature overnight. Lastly, the solution underwent three 30-min dialysis processes using a 12000 Da dialysis bag. IR (KBr, cm^{-1}): 3700-3000, 2926, 2856, 1744, 1608, 1476, 1150-1060, 544.

Synthesis of Fl@p(Hist-CA)

To a Fl (5 mg, 15 µmol) solution in 10 ml of ethanol, 7.3 µL of TO was added, and the mixture was homogenized in an ultrasonic bath. Then ethanol was distilled off under reduced pressure. Hist-RA (2.67 mg, 2 µmol) and CA-RA (5.95 mg, 4.4 µmol) in 1 mL of double-distilled water and BA (0.6 mg, 5 mmol) in 4 mL of PB (pH 8.5) were added. The mixture was vortexed at 3500 rpm for one minute until an emulsion formed. The solution was then purged with argon in an ultrasonic bath for 90 minutes. The solution was stirred at room temperature overnight and then purified by dialysis using a 12000 Da dialysis bag.

The amount of encapsulated Fl was determined by UV spectroscopy at 487 nm (ε = 83000 M^{-1}×cm^{-1}).

EE% was calculated as the ratio of the mass of encapsulated Fl to the initially taken quantity:

$$EE\% = \frac{m_{Fl}}{m_{Fl}^0} \times 100\,\% \tag{1}$$

where m_{Fl} is the mass of encapsulated Fl, mg; m_{Fl}^0 is the mass of Fl taken for the

reaction, mg.

Synthesis of Atr@p(Hist-CA) and Atr release under ACh influence

Atr@p(Hist-CA) was synthesized, similar to Fl@p(Hist-CA), using 10 mg (25.8 μmol)

of atropine sulfate.

The resulting Atr@p(Hist-CA) solution underwent purification through a single

1.5 h dialysis process using a 12,000 Da dialysis bag. The dialysate was then

evaporated under reduced pressure. The residue was dissolved in 650 μL of D2O with

0.04% DMF. The unencapsulated Atr amount was determined by the ratio of the DMF

signal intensity at 7.91 ppm to the Atr signal at 5.05 ppm.

ACh (4.54 mg, 25 μmol) was introduced to the prodilyzed purified Atr@p(Hist-

CA) solution, followed by another 1.5 h dialysis. The resulting dialysate underwent

evaporation under reduced pressure, and the residue was again dissolved in 650 μL

of 0.04% DMF in D2O. The released Atr amount was also calculated by the ratio of the

DMF signal intensity at 7.91 ppm to the Atr signal at 5.05 ppm.

The solvent in the dialyzed solution was evaporated under reduced pressure,

and the residue was dissolved in 0.04% DMF in D$_2$O. The analysis of the unreleased

Atr amount was conducted similarly to the method described in the prior paragraphs.

Cytotoxicity

Based on fluorescence intensity, the cytotoxic effect was determined using the Cell

Viability BioApp on the Cytell Cell Imaging multifunctional system (GE Healthcare Life

Science, Sweden) [38]. The experiments utilized a Chang liver cell line (human liver

cells) from the N. F. Gamaleya National Research Center for Epidemiology and Microbiology and a cell culture of WI-38 VA 13 subline 2RA (human embryo lung) from the Collection of the Institute of Cytology RAS (St. Petersburg). Standard culture media Igla, produced by the Moscow Institute of Poliomyelitis and Viral Encephalitis, named after the M.P. Chumakova firm PanEco and was employed for cell culture, supplemented with 1% nonessential amino acids (NEAA) and 10% fetal bovine serum. The cells were grown in a CO2 incubator at 37°C after being seeded on a 96-well Eppendorf plate at a concentration of 100 000 cells/mL per well in 150 μL of medium. After 24 hours of incubation, 150 μL of the tested dispersions were added to each well. Twice dilutions of the dispersions were prepared directly in the growth medium.

Hemocompatibility

Human erythrocytes were obtained at medical office of the A. E. Arbuzov Institute of Organic and Physical Chemistry from two Caucasian volunteers (52 years old, blood group II and 24 years old, blood group IV), after receiving informed consent. The study was approved by the ethical committee of the FRC Kazan Scientific Center of RAS according to Russian national ethical guidelines (protocol No. 9–2013). No organs/tissues were procured from prisoners.

Hemolysis of Human Red Blood Cells (hRBC)

The hemolytic activity of Hist-RA, CA-RA, and p(Hist-CA) were evaluated against hRBC [38]. Following a 10-minute, 800-rpm centrifugation of fresh hRBC with EDTA, the cells were three times washed with PBS (35 mM PB/0.15 M NaCl, pH 7.3) before being resuspended in PBS. Then, 0.5 mL of a hRBC stock solution in PBS was mixed with samples dissolved in PBS to reach a final volume of 5 mL (final erythrocyte concentration, 10% v/v). The resultant suspension was agitated and incubated at 37 °C for one hour. After that, the samples were centrifuged for 10 minutes at 2000 rpm.

The absorbance of the supernatant at 540 nm was used to calculate the amount of hemoglobin that had been liberated. Controls for zero hemolysis (blank) and 100 % hemolysis consisted of hRBC suspended in PBS and distilled water, respectively. The experiments were repeated three times.

Hemagglutination test

The human erythrocytes (groups II and IV) were utilized in the study. The erythrocytes underwent two washes with 0.9% saline solution and were centrifuged at 2500 g for 10 minutes at 4°C. Following each centrifugation cycle, the supernatant was meticulously discarded. Subsequently, the red blood cells were resuspended in 0.9% saline to achieve a concentration of 2%. The hemagglutination activity of the test compounds was examined in a 96-well U-microtiter plate. Subsequently, two-fold serial dilutions of the studied compositions were prepared. 100 µL of each dilution was combined with 100 µL of 2% packed red blood cells (1:1) and added to a well of a 96-well U microtiter plate. Each dilution was tested in 2 parallel wells. The samples were then an incubated for 1 hour at 37°C, followed by hemagglutination observation with the naked eye (Figure 3) [39]. Images of the samples were captured using a Nikon Eclipse Ci-S microscope (Nikon, Japan) (Figure 4).

Supporting Information

^{1}H and ^{13}C NMR spectra of Hist-RA and CA-RA; and hemolytic activity of Hist-RA, CA-RA and p(Hist-CA).

File Name: SI

File Format: pdf

Title: Nanocarrier containing carboxylic and histamine groups with dual action: acetylcholine hydrolysis and antidote Atropine delivery

Acknowledgements

Funding

References

1. Lott, E. L.; Jones, E. B, Cholinergic Toxicity. In: *StatPearls* [Internet] Publishing. Treasure Island (FL): https://www.ncbi.nlm.nih.gov/books/NBK539783/ (accessed Jan, 2024).

2. Jett, D. A., Guignet, M.; Supasai, S.; Lein, P. J. Developmental Toxicity Within the Central Cholinergic Nervous System. In *Handbook of Developmental Neurotoxicology*, 2nd ed.; Slikker, W.; Paule, M. G.; Wang, C., Ed.; Academic Press: Cambridge, 2018, pp 183-198. https://doi.org/10.1016/B978-0-12-809405-1.00016-X

3. Cummings, J. L. *Am. J. Geriatr. Psychiatry* **2003**, *11*, 131-145. https://doi.org/10.1097/00019442-200303000-00004

4. Leikin, J. B.; Braund, V.; DesLauris, C. *Am. J. Emerg. Med.* **2014**, *32*, 815.e3-815.e4. https://doi.org/10.1016/j.ajem.2013.12.048

5. Mukherjee, S.; Gupta, R. D. *J. Toxicol.* **2020**, *2020*, 3007984. https://doi.org/10.1155/2020/3007984

6. Robenshtok, E.; Luria, S.; Tashma, Z.; Hourvitz, A. *Isr. Med. Assoc. J.* **2002**, *4*, 535–539.

7. Bardin, P. G.; Van Eeden, S. F. *Crit. Care Med.* **1990**, *18*, 956–960.

8. Arendse, R.; Irusen, E. *Hum. Exp. Toxicol.* **2009**, *28*, 715–720. https://doi.org/10.1177/0960327109350666

9. Zhang, H.; Zhang, M.; Du, Y.; He, J.; Li, J. *Medicine* **2023**, *102*, e34775. https://doi.org/10.1097/md.0000000000034775

10. Kaiti, R. *Beyoglu Eye J.* **2022**, *7*, 157–166. https://doi.org/10.14744/bej.2022.07742

11. Addo, R. T.; Yeboah, K. G.; Siwale, R. C.; Siddig, A.; Jones, A.; Ubale, R. V.; Akande, J.; Nettey, H.; Patel, N. J.; Addo, E.; D'Souza, M. J. *J. Pharm. Sci.* **2015**, *104*, 1677–1690. https://doi.org/10.1002/jps.24380

12. Claßen, R.; Pouokam, E.; Wickleder, M.; Diener, M.; Mattern, A. *R. Soc. Open Sci.* **2022**, *9*, 220244. https://doi.org/10.1098/rsos.220244

13. Yu, G.; Chen, X. *Theranostics* **2019**, *9*, 3041–3074. https://doi.org/10.7150/thno.31653

14. Castillo-Aguirre, A.; Esteso, M. A.; Maldonado, M. *Curr. Org. Chem.* **2020**, *24*, 2412–2425. https://doi.org/10.2174/1385272824999200510232141

15. Pashirova, T. N.; Zhil´Tsova, E. P.; Lukashenko, S. S.; Gibadullina, E. M.; Burilov, A. R.; Zakharova, L. Ya.; Konovalov, A. I. *Russ. Chem. Bull.* **2016**, *65*, 1272–1277. https://doi.org/10.1007/s11172-016-1447-3

16. Ryzhkina, I. S.; Pashirova, T. N.; Habicher, W. D.; Kudryavtseva, L. A.; Konovalov, A. I. *Macromol. Symp.* **2004**, *210*, 41–48. https://doi.org/10.1002/masy.200450605

17. Cuevas, F.; Di Stefano, S.; Magrans, J. O.; Prados, P.; Mandolini, L.; De Mendoza, J. *Chem. Eur. J.* **2000**, *6*, 3228–3234. https://doi.org/10.1002/1521-3765(20000901)6:17

18. Ziganshina, A. Yu.; Mansurova, E. E.; Antipin, I. S. *Colloid J.* **2022**, *84*, 518–529. https://doi.org/10.1134/s1061933x22700028

19. Voloshina, A. D.; Mansurova, E. E.; Bakhtiozina, L. R.; Shulaeva, M. M.; Nizameev, I. R.; Lyubina, A. P.; Amerhanova, S. K.; Kadirov, M. K.; Ziganshina, A. Y.; Semenov, V. E.; Antipin, I. S. *New J. Chem.* **2022**, *46*, 12572–12580. https://doi.org/10.1039/d2nj02059a

20. Sultanova, E. D.; Krasnova, E. G.; Kharlamov, S. V.; Nasybullina, G. R.; Yanilkin, V. V.; Nizameev, I. R.; Kadirov, M. K.; Mukhitova, R. K.; Zakharova, L. Y.; Ziganshina, A. Y.; Konovalov, A. I. *ChemPlusChem* **2014**, *80*, 217–222. https://doi.org/10.1002/cplu.201402221

21. Sultanova, E. D.; Atlanderova, A. A.; Mukhitova, R. D.; Salnikov, V. V.; Osin, Y. N.; Ziganshina, A. Y.; Konovalov, A. I. *RSC Adv.* **2016**, *6*, 70072–70076. https://doi.org/10.1039/c6ra15165e

22. Ziganshina, A. Y.; Mansurova, E. E.; Shulaeva, M. M.; Syakaev, V. V.; Semenov, V. E.; Antipin, I. S. *Molbank* **2022**, *2022*, M1507. https://doi.org/10.3390/m1507

23. Murayama, K.; Aoki, K. *Chem. Commun.* **1997**, No. 1, 119–120. https://doi.org/10.1039/a607131g

24. Demura, M.; Yoshida, T.; Hirokawa, T.; Kumaki, Y.; Aizawa, T.; Nitta, K.; Bitter, I.; Tóth, K. *Bioorg. Med. Chem. Lett.* **2005**, *15*, 1367–1370. https://doi.org/10.1016/j.bmcl.2005.01.012

25. Ballester, P.; Sarmentero, M. A. *Org. Lett.* **2006**, *8*, 3477–3480. https://doi.org/10.1021/ol061097i

26. Salorinne, K.; Tero, T.-R.; Riikonen, K.; Nissinen, M. *Org. Biomol. Chem.* **2009**, *7*, 4211. https://doi.org/10.1039/b911389d

27. Inouye, M.; Hashimoto, K.-I.; Isagawa, K. *J. Am. Chem. Soc.* **1994**, *116*, 5517–5518. https://doi.org/10.1021/ja00091a085

28. De Boer, D.; Nguyen, N.; Mao, J.; Moore, J.; Sorin, E. J. *Biomolecules* **2021**, *11*, 580. https://doi.org/10.3390/biom11040580

29. Sergeeva, T. Yu.; Nizameev, I. R.; Kholin, K. V.; Kadirov, M. K.; Samigullina, A. I.; Gubaidullin, A. T.; Mukhitova, R. K.; Ziganshina, A. Yu.; Antipin, I. S. *Russ. Chem. Bull.* **2020**, *69*, 351–359. https://doi.org/10.1007/s11172-020-2767-x

30. Luostarinen, M.; Nissinen, M.; Nieger, M.; Shivanyuk, A.; Rissanen, K. *Tetrahedron* **2007**, *63*, 1254–1263. https://doi.org/10.1016/j.tet.2006.11.044

31. Beyeh, N. K.; Cetina, M.; Löfman, M.; Luostarinen, M.; Shivanyuk, A.; Rissanen, K. *Supramol. Chem.* **2010**, *22*, 737–750. https://doi.org/10.1080/10610278.2010.506543

32. Elzayat, A.; Adam-Cervera, I.; Álvarez-Bermúdez, O.; Muñoz-Espí, R. *Colloids Surf. B* **2021**, *203*, 111764. https://doi.org/10.1016/j.colsurfb.2021.111764

33. Chaleshtari, Z. A.; Zhou, M.; Foudazi, R. *J. Appl. Phys.* **2022**, *131*. https://doi.org/10.1063/5.0081303

34. Sergeeva, T. Yu.; Mukhitova, R. K.; Nizameev, I. R.; Kadirov, M. K.; Sapunova, A. S.; Voloshina, A. D.; Mukhametzyanov, T. A.; Ziganshina, A. Y.; Antipin, I. S. *ChemPlusChem* **2019**, *84*, 1560–1566. https://doi.org/10.1002/cplu.201900428

35. Sergeeva, T. Yu.; Mukhitova, R. K.; Bakhtiozina, L. R.; Nizameev, I. R.; Kadirov, M. K.; Sapunova, A. S.; Voloshina, A. D.; Ziganshina, A. Y.; Antipin, I. S. *Supramol. Chem.* **2020**, *32*, 150–161. https://doi.org/10.1080/10610278.2020.1714620

36. Lurie, J. Handbook of Analytical Chemistry; Goskhimizdat: Moscow, Soviet Union, 1975.

37. Gibb, B. C.; Chapman, R. G.; Sherman, J. C. *J. Org. Chem.* **1996**, *61*, 1505–1509. https://doi.org/10.1021/jo951633c

38. Voloshina, A. D.; Semenov, V. E.; Strobykina, A. S.; Kulik, N. V.; Krylova, E. S.; Zobov, V. V.; Reznik, V. S. *Russ. J. Bioorg. Chem.* **2017**, *43*, 170–176. https://doi.org/10.1134/s1068162017020170

39. Banerjee, N.; Sengupta, S.; Roy, A.; Ghosh, P.; Das, K.; Das, S. *PloS One* **2011**, *6*, e18593. https://doi.org/10.1371/journal.pone.0018593